

Modelling impacts of tidal stream turbines on surface waves

Xiaorong Li¹, Ming Li², Stuart McLelland³, Laura-Beth Jordan³,
Laurent O. Amoudry⁴, Qingyang Song⁵, Andy Plater¹

¹School of Environmental Sciences, University of Liverpool, Liverpool L69
7ZT, UK,

²School of Engineering, University of Liverpool, Liverpool L69 3GQ, UK

³School of Environmental Sciences, University of Hull, Cottingham Road,
Hull HU6 7RX, UK

⁴National Oceanography Centre, Joseph Proudman Building, 6 Brownlow
Street, Liverpool L3 5DA, UK

⁵FTZ-Westkste/Coastal Research Laboratory,
Christian-Albrechts-Universitt zu Kiel, Kiel, Germany

Abstract

A high resolution Computational Flow Dynamics (CFD) numerical model is built based on a laboratory experiment in this research to study impacts of tidal turbines on surface wave dynamics. A reduction of $\sim 3\%$ in wave height is observed under the influence of a standalone turbine located 0.4 m from the free surface. The artificial wave energy dissipation routine ‘OBSTACLE’ within FVCOM is shown to effectively capture the correct level of wave height reduction, reproducing the CFD results with significantly less computational effort.

The turbine simulation system is then applied to a series of test cases to investigate impact of a standalone turbine on bed shear stress. Results suggest an apparent increase in bed stress ($\sim 7\%$) upstream of the turbine due to the inclusion of surface waves. However, in the immediate wake of the turbine, bed stress is dominated by the presence of the turbine itself, accounting for a $\sim 50\%$ increase, with waves having a seemingly negligible effect up to 9D downstream of the turbine. Beyond this point, the effect of waves on bed shear stress become apparent again. The influence of OBSTACLE on bed stress is also noticeable in the far wake, showing a reduction of $\sim 2\%$ in wave height.

1 Introduction

As a very promising clean, non-carbon alternative to traditional fossil fuels, tidal stream energy has been gaining significant attention. However, despite

4 the growing interest in this sector of renewable energy, our understanding of
5 the impacts of tidal stream energy devices on the surrounding environment
6 is still limited, largely due to the lack of data collected from on-site projects.

7 Alternatively, laboratory experiments and numerical simulations are widely
8 adopted to investigate such impacts. For example, porous actuator disc sim-
9 ulators [1, 2, 3] and down-scaled turbine prototype models [4, 5] have been
10 used in laboratories to study turbine-caused impacts on passing flows and
11 turbulence. Also, [6] carried out laboratory experiments to study changes of
12 wake recovery of a turbine subjected to opposing waves. As a complement
13 to laboratory experiments, Computational Flow Dynamics (CFD) modelling
14 is also commonly applied. Similarly, works with turbines approximated as
15 porous discs [7, 8, 9] and with realistic turbine geometry resolved in the com-
16 putational mesh [10, 11, 12] have been published to reveal how flow patterns
17 and turbulent mixing are changed by the turbine in near-field scale.

18 To study the far-field hydrodynamic changes caused by the operation
19 of turbines and turbine arrays, numerical oceanographic models, such as
20 Regional Ocean Modelling System (ROMS) [13] and The Unstructured Grid
21 Finite Volume Community Ocean Model (FVCOM) [14], have also been used.
22 Modifications have been made to such models in order to simulate the effect
23 of tidal stream turbines on the flow motion. These modifications are mostly
24 based on either the additional bottom friction approach [15, 16, 17] or the
25 turbine-induced body force concept [18, 19, 20, 21, 22, 23, 24].

26 In an effort to account for turbine-caused impacts on turbulence in large
27 scale oceanographic models, [25] added three terms to the $k-\epsilon$ closure within
28 ROMS to model turbine related turbulence generation, dissipation and tur-
29 bulence length-scale interference. These three terms were later adapted ac-
30 cordingly to accommodate the theory around which the MY-2.5 turbulence
31 closure is based and applied in FVCOM by [26].

32 In terms of interactions between surface waves and tidal turbines, current
33 research focus has been mainly put on the impact of waves on the performance
34 of turbines due to its immediate industry relevance [27, 28, 29, 30, 31, 32, 33].
35 However, there is a lack of emphasis on the effects of turbines on surface waves
36 in both physical experimental studies and numerical modelling. Because tidal
37 turbines are normally expected to be installed in relatively shallow coastal
38 waters due to difficulties in device installation and operation that would oc-
39 cur otherwise [2], they are likely to have a close proximity to the free surface
40 and hence interfere with the propagation of surface waves. Also, the altered
41 three-dimensional flow structure due to the presence of tidal turbines could

42 also have influence on surface waves through wave-current interaction mech-
43 anisms. Surface waves, particularly in shallow coastal areas, can influence
44 sediment transport dynamics significantly. For instance, vertical mixing in
45 the water column due to wave activities can keep sediment in suspension for
46 longer, inhibiting sediment deposition in the downstream areas of the turbine
47 [34]. Also, wave actions can increase bottom shear stress, leading to enhanced
48 sediment resuspension and erosion [35]. Further, through wave-current in-
49 teractions, waves can drive longshore currents, contributing to long-term
50 shoreline evolution [36, 37]. Therefore, changes in wave dynamics caused by
51 tidal turbines are of high importance in terms of fully understanding impact
52 of tidal turbines on local and regional geomorphology.

53 Due to the aforementioned interactions, the primary objectives of the
54 work documented in this paper are to first explore the potential impacts
55 of tidal turbines on surface waves with the help of high resolution CFD
56 simulations, and second, to develop a Horizontal Axis Tidal Turbine (HATT)
57 simulation system that could implement the impacts of tidal stream turbines
58 on surface waves with a realistic spatial scale.

59 This paper details one high resolution CFD model for tidal turbine im-
60 pact assessment on surface waves. Understandings obtained from the CFD
61 modelling then advise turbine parameterization in large scale oceanographic
62 models. The high resolution modelling is based on a CFD solver — AN-
63 SYS FLUENT. The implementation of effects of turbine operation on sur-
64 face waves is an extension of the turbine simulation platform reported in
65 [26], which parameterized tidal turbines in the current and turbulence clo-
66 sure modules of FVCOM. Impacts of tidal turbines on surface waves are
67 considered in this new model by modification of wave energy flux across the
68 device. A thorough validation study is also presented in which the turbine
69 representation and operation in the CFD models is validated against labora-
70 tory data collected from an experiment conducted at the University of Hull
71 using their ‘Environment Simulator Laboratory Flume’ [5] and the FVCOM
72 model is verified utilizing the CFD simulated results.

73 The structure of the paper is provided as follows for clarity. Firstly in
74 Section 2 ANSYS FLUENT and the FVCOM model are introduced. The in-
75 tegration of turbine simulation within these two frameworks is also discussed
76 in this section. Next, Section 3 introduces the exploratory CFD models which
77 aim to reveal the impacts of turbines on surface waves. A set of experimental
78 data was used for CFD model validation in this section. Section 4 details the
79 verification study for the turbine implementation in FVCOM which considers

80 surface waves. Note that as the experimental data available was considered
 81 insufficient for comprehensive validation, verification in this section is based
 82 on data generated via the CFD modelling detailed in Section 3. In Section 5,
 83 the turbine simulation system developed based on FVCOM is applied to test
 84 cases in order to reveal impacts of a standalone turbine on its surroundings
 85 which incorporate wave-current interaction processes. A set of discussion is
 86 presented in Section 6, followed by concluding remarks given in Section 7 to
 87 summarise important results from sections 4 and 5, along with suggestions
 88 for potential future developments.

89 2 Modelling system

90 2.1 ANSYS FLUENT — a CFD solver

91 FLUENT solves the three-dimensional Reynolds-averaged Navier-Stokes (RANS)
 92 equations which can be written in tensor form as follows:

$$\frac{\partial \rho}{\partial t} + \frac{\partial \rho \bar{u}_i}{\partial x_i} = 0 \quad (1)$$

93

$$\frac{\partial(\rho \bar{u}_i)}{\partial t} + \frac{\partial(\rho \bar{u}_i \bar{u}_j)}{\partial x_j} = -\frac{\partial \bar{P}}{\partial x_i} + \frac{\partial}{\partial x_j} \left[\mu \left(\frac{\partial \bar{u}_i}{\partial x_j} + \frac{\partial \bar{u}_j}{\partial x_i} \right) - \frac{2}{3} \mu \frac{\partial u_j}{\partial x_i} \delta_{ij} \right] + \frac{\partial}{\partial x_j} (-\rho \overline{u_i' u_j'}) + F_i \quad (2)$$

94 where ρ is the water density; t is time; μ is the molecular viscosity; δ_{ij} is the
 95 Kronecker delta and F_i are external body forces in the i directions (x, y, z).
 96 \bar{u}_i ($\bar{u}, \bar{v}, \bar{w}$) and u_i' (u', v', w') are the time-averaged (mean) and fluctuating
 97 water velocities in the x_i (x, y, z) directions, respectively. The combination
 98 of these two velocity components forms the instantaneous (exact) velocities:

$$u_i = \bar{u}_i + u_i' \quad (3)$$

99 Likewise, \bar{P} is the time-averaged static pressure and for all scalar vari-
 100 ables:

$$\phi = \bar{\phi} + \phi' \quad (4)$$

101 where ϕ denotes a scalar quantity such as pressure and $\bar{\phi}$ and ϕ' are the mean
 102 and fluctuating components of a scalar variable.

103 The Reynolds stress terms, $-\rho \overline{u_i' u_j'}$, which appear on the right hand side
 104 of Equation 2 represent the effects of turbulence and are modelled based

105 on the Shear Stress Transport (*SST*) $k - \omega$ turbulence closure [38] in this
 106 research.

107 To simulate the wind-wave-induced free surface effects, the Volume of
 108 Fluid (VOF) method is used in FLUENT. The formulation of the VOF model
 109 relies on the fact that the modelled phases are not immiscible. It calculates
 110 the fractions (α_i , $0 < \alpha_i < 1$) of the simulated phases (water and air in
 111 the present research) in each computational cell and in each control volume.
 112 The volume fractions of all phases sum to unity. Based on the local value of
 113 α_i , the appropriate properties and variables will be assigned to each control
 114 volume within the domain.

115 A single momentum equation which is dependent on the volume fractions
 116 of all phases through the properties ρ and μ is solved throughout the calcu-
 117 lation domain, and the computed velocity field is shared among the phases.
 118 The momentum equation is given by

$$\frac{\partial}{\partial t}(\rho\vec{v}) + \nabla \cdot (\rho\vec{v}\vec{v}) = -\nabla p + \nabla \cdot [\mu(\nabla\vec{v} + \nabla\vec{v}^T)] + \rho\vec{g} + \vec{F} \quad (5)$$

119 where ρ is the volume-fraction-averaged density $\rho = \sum \alpha_i \rho_i$ and μ the
 120 volume-fraction-averaged viscosity calculated in the same manner.

121 A continuity equation for the volume fraction of one (or more) of the
 122 phases helps to track the interface(s) between the phases. For the i^{th} phase,
 123 this equation takes the form of the following:

$$\frac{\partial \alpha_i}{\partial t} + \vec{v} \cdot \nabla \alpha_i = 0 \quad (6)$$

124 Additional scalar equations, such as those solving turbulence quantities,
 125 are also processed applying the shared-fields approach; i.e. only a single/a
 126 single set of transport equations is solved and the variables (e.g., k and ω)
 127 are shared by the phases throughout the domain.

128 A wave boundary condition is applied to the velocity inlet of the VOF
 129 model to enable the simulation of wave propagation. FLUENT provides
 130 a good variety of wave theories such as first order linear wave theory and
 131 second/higher order Stokes wave theories. The choice of wave theory is
 132 made based on Ursell number ($U_r = \frac{HL^2}{d^3}$) and wave steepness (H/L), where
 133 H , L and d are wave height, wave length and water depth, respectively.
 134 Linear wave theory is suitable when $U_r < 40$, given $H/L < 0.04$ and sec-
 135 ond/higher order Stokes wave theories are more appropriate when $U_r < 40$
 136 and $H/L > 0.04$ [39]. The wave theories are fully coupled with the continuity

137 and momentum equations of FLUENT. Details of the wave theories and the
 138 wave-current coupling can be found in [38, 40].

139 **2.2 Representation of HATT in FLUENT**

140 The Virtual Blade Model (VBM) is adopted in this research to simulate
 141 HATT in FLUENT. In VBM, the actual blades are not directly present.
 142 Instead, the rotor is simulated inside a rotor disk fluid zone across which the
 143 virtual blades swipe. The virtual blades are achieved through adding a body
 144 force in the x , y and z directions. This method is an application of a built-in
 145 blade simulating scheme — Blade Element Method (BEM) — within ANSYS
 146 FLUENT. In BEM, each blade is divided into small sections from root to tip.
 147 The lift and drag forces exerted on each segment are calculated based on the
 148 blade design as well as the lift and drag coefficients of each section:

$$f_{L,D} = c_{L,D} \cdot c(r/R) \cdot \frac{\rho \cdot V_{tot}^2}{2} \quad (7)$$

149 where $c_{L,D}$ is lift/drag coefficient specified by the user; $c(r/R)$ is the chord
 150 length; ρ is the fluid density and V_{tot} is the fluid velocity relative to the blade.

151 The lift and drag forces are then averaged over a full turbine rotation to
 152 calculate the force on each cell in the discretized domain:

$$F_{L,D_{cell}} = N_b \cdot \frac{dr \cdot d\theta}{2\pi} \cdot f_{L,D} \quad (8)$$

153

$$\vec{S}_{cell} = -\frac{\vec{F}_{cell}}{V_{cell}} \quad (9)$$

154 where N_b is the number of blades and V_{cell} is the volume of a grid cell.

155 **2.3 Three-dimensional FVCOM**

156 To model the impacts of tidal stream energy devices on coastal regions, FV-
 157 COM, which is a three-dimensional, free surface, terrain-following oceanographic
 158 model [14], is used in this research. The momentum and continuity
 159 equations of FVCOM are presented in Equations 10-13. FVCOM includes
 160 fully coupled wave-current-sediment modules and, therefore, is particularly
 161 useful for modelling coastal processes. Also, it uses an unstructured trian-
 162 gular mesh to discretize computational domains horizontally, which allows

163 for high resolution around individual turbines whilst maintaining a smooth
 164 transition to a relatively large mesh size far from the turbines. Such a treat-
 165 ment of spatial discretization provides a good balance between accuracy and
 166 computational effort.

$$\frac{\partial u}{\partial t} + u \frac{\partial u}{\partial x} + v \frac{\partial u}{\partial y} + w \frac{\partial u}{\partial z} - f v = -\frac{1}{\rho} \frac{\partial(P_H + P_a)}{\partial x} - \frac{1}{\rho} \frac{\partial q}{\partial x} + \frac{\partial}{\partial z} \left(K_m \frac{\partial u}{\partial z} \right) + F_u \quad (10)$$

167

$$\frac{\partial v}{\partial t} + u \frac{\partial v}{\partial x} + v \frac{\partial v}{\partial y} + w \frac{\partial v}{\partial z} + f u = -\frac{1}{\rho} \frac{\partial(P_H + P_a)}{\partial x} - \frac{1}{\rho} \frac{\partial q}{\partial y} + \frac{\partial}{\partial z} \left(K_m \frac{\partial v}{\partial z} \right) + F_v \quad (11)$$

168

$$\frac{\partial w}{\partial t} + u \frac{\partial w}{\partial x} + v \frac{\partial w}{\partial y} + w \frac{\partial w}{\partial z} = -\frac{1}{\rho} \frac{\partial q}{\partial z} + \frac{\partial}{\partial z} \left(K_m \frac{\partial w}{\partial z} \right) \quad (12)$$

169

$$\frac{\partial u}{\partial x} + \frac{\partial v}{\partial y} + \frac{\partial w}{\partial z} = 0 \quad (13)$$

170 where x , y , and z are the east, north, and vertical axes in the Cartesian
 171 coordinate system; u , v , and w are the three velocity components in the x ,
 172 y , and z directions respectively; P_a is the air pressure at sea surface; P_H
 173 is the hydrostatic pressure; q is the non-hydrostatic pressure; f is the Coriolis
 174 parameter and K_m is the vertical eddy viscosity coefficient. F_u , F_v represent
 175 horizontal momentum terms.

176 Extensive work has been done by the authors to enable the prediction of
 177 complete three-dimensional velocity profiles and mixing in the wake of tur-
 178 bines by making modifications to the current and turbulence closure modules
 179 of FVCOM [26]. The current research further extends the turbine simula-
 180 tion platform reported in [26] in terms of proposing a way to incorporate the
 181 effects of turbines on surface waves in the model.

182 For completeness, the basic theory surrounding surface waves and wave-
 183 current coupling in FVCOM is given as follows. More details of the model
 184 can be found in [41].

185 To simulate surface wave propagation, Simulating Waves Nearshore (SWAN)
 186 [42] is integrated with FVCOM. The governing equation of the wave action
 187 density spectrum is given as:

$$\frac{\partial N}{\partial t} + \nabla \cdot \left[\left(\vec{C}_g + \vec{V} \right) N \right] + \frac{\partial C_\sigma N}{\partial \sigma} + \frac{\partial C_\theta N}{\partial \theta} = \frac{S_{tot}}{\sigma} \quad (14)$$

188 where N is the wave action density spectrum, \vec{C}_g is the group velocity vector,
 189 \vec{V} is the ambient water current vector, σ is the relative frequency, θ is the wave

190 direction, C_σ and C_θ are the wave propagation velocities in the frequency
191 domain and directional space respectively and S_{tot} is the source-sink term
192 considering wind-induced wave growth, nonlinear transfer of wave energy due
193 to three-wave interactions, nonlinear transfer of wave energy due to four-wave
194 interactions, wave decay due to white capping, wave decay due to bottom
195 friction and wave decay due to depth-induced wave breaking. More details
196 are available in the SWAN technical manual [42].

197 Due to the presence of surface waves, the bottom boundary layer is af-
198 fected and the shear stress is much higher than that due to current alone
199 [35]. To take this into account, a special treatment is needed close to the
200 bed, which is implemented in the bottom boundary layer module (BBL).
201 BBL calculates the bottom shear stresses under the condition of combined
202 waves and currents. The calculation of bottom shear stress is important as
203 it influences the flow field as well as sediment transport patterns. The BBL
204 module developed by [43] based on the theory proposed by [44] was con-
205 verted into an unstructured-grid finite-volume version and implemented in
206 FVCOM. It is, hence, used in the present research. Details of BBL can be
207 found in [43].

208 FVCOM includes a wave-current-sediment fully coupled system. After
209 initialization, the wave module starts to solve the wave dynamics, providing
210 information of surface waves. The interactions between the current and wave
211 modules are achieved through radiation stress terms according to Mellor’s
212 theory [45, 46, 47]. Results from the current module, velocities and surface
213 elevation in particular, provide the wave module feedback for the next time
214 step calculation. Results from the current and wave modules are then sent
215 to the BBL module to calculate the bottom stresses under the combined
216 influence of waves and current. These stresses are then used to solve the
217 momentum equations.

218 **2.4 Representation of HATT in FVCOM**

219 As will be demonstrated by CFD experiments in Section 3, surface wave
220 height is affected by the inclusion of turbines. To represent this effect, one
221 of the built-in features of SWAN — “OBSTACLE” is applied in the present
222 study. The OBSTACLE routine absorbs wave energy along a finite line
223 (defined between two locations) and dissipates it according to a constant
224 transmission coefficient K_t . A detailed implementation of the OBSTACLE
225 routine in this context can be found in [48].

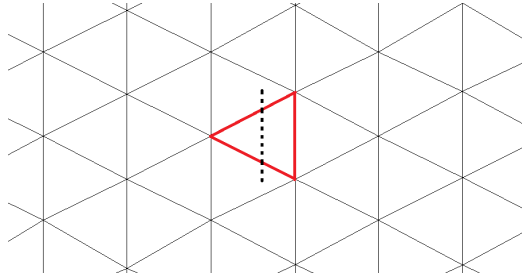


Figure 1: Illustration of the turbine position in the x-y plane on the mesh. The red triangle indicates the mesh element in which the turbine is implemented. The black dotted line illustrates the application of OBSTACLE.

226 To model the effect of turbines on waves, the OBSTACLE energy absorp-
 227 tion line length in the model is set to the diameter of the simulated turbine.
 228 Note however that the impact of the line length upon the simulation is not
 229 continuous, as it absorbs energy only where it intersects with the mesh. In
 230 other words, two energy absorption lines of different length but with ends
 231 lying in the same respective triangle segments would have equal effect. The
 232 line is positioned in a way that it passes through the centre and crosses two
 233 sides of the triangles selected to house the turbine (see Figure 1). It should
 234 be pointed out that the turbine parameterization in the current and turbu-
 235 lence closure modules of FVCOM reported in [26] are utilized in this research
 236 when a turbine is present.

237 3 The CFD model

238 A CFD model is built in this research to study the impacts of tidal turbines
 239 on surface waves. It is based on an experiment carried out at the University
 240 of Hull using their ‘Environment Simulator Laboratory Flume’ [5]. The flume
 241 is 11 m in length, 1.6 m wide and 0.8 m deep. The water depth was 0.6m
 242 throughout the experiment. The flow rate at the inlet was 0.3 m/s. A surface
 243 wave propagating in the direction of the flow was imposed upon the inlet. The
 244 wave height and wave period were 0.15 m and 1 s, respectively. A horizontal
 245 axis rotor with a diameter of 0.2 m was located 0.2 m above the bed and
 246 the tip speed ratio (TSR) of the rotor was constantly 5.5. Measurements of
 247 velocity were taken along the centreline from 1D to 4D downstream of the
 248 rotor (where D is the turbine diameter).

249 Although a wide range of data was collected, the measurements did not
250 include free surface variations which are the main focus of this research.
251 Therefore, a CFD model replicating the experimental conditions was set up
252 to capture the impacts of the rotor on surface waves. The CFD model was
253 validated by recreating the conditions of the experiments for which measure-
254 ments were available.

255 In the CFD model, the flume length was, instead of 11m, 3.1 m for ease
256 of simulation. The velocity at the inlet was 0.3 m/s. A following wave with
257 wave height of 0.15 m and wave period of 1 s was imposed at the inlet. The
258 computation of wave propagation is based on the 2nd-order wave theory. To
259 reduce the wave energy being reflected back into the flume from the exit,
260 three porous zones, with thickness of 0.2m, 0.2m and 0.1m, were set at the
261 outlet boundary, with porosity declining from 0.95 to 0.9 to 0.8. Essential
262 configurations of VBM, i.e. geometrical setup and running parameters of the
263 rotor are specified according to [49].

264 Figure 2 compares the ensemble average of stream-wise flow velocity pro-
265 files predicted by the CFD model against that measured in the laboratory at
266 1D, 2D, 3D and 4D downstream of the rotor. It should be noted that there
267 are overlaps in the measured profiles. This is because in the laboratory, the
268 centreline slice on which the velocities were measured was divided into 9 sub-
269 slices and each of these sub-slices overlaps with its neighbour sub-slices. The
270 overlaps provide a way to ensure the sub-slices are aligned correctly.

271 It can be seen from Figure 2 that the computed velocity profiles at all 4
272 locations agree well with the measurements at the rotor swiping layers with
273 the exception of location 1D specifically above the rotor hub. This is due
274 to the fact that the rotor housing and supporting structure (suspending the
275 turbine from above) in the laboratory flume interfere with the flow at 1D.
276 As these additional structures are not accounted for in the model, the result
277 differs in this area. Further, the velocities in the region below the rotor are
278 over-estimates. This over-estimation is likely due to a slightly over-predicted
279 near bed wave boundary layer effect. To quantify the agreement between the
280 predictions and measurements, the Nash Sutcliffe Model Efficiency (NSME)
281 is calculated based on Equation 15 for each location for the rotor swiping
282 layers and provided in Table 1. The NSME has been widely used to quantify
283 the accuracy of model prediction, and the model performance is considered
284 as excellent for NSME in between 0.65-1, very good for 0.65-0.5, good for
285 0.5-0.2, and poor for less than 0.2 (e.g. [50, 51, 52]). Therefore, the agree-
286 ment between FLUENT based CFD model results and measured data are

Table 1: NSME for the CFD case against the experimental data

1D	2D	3D	4D
0.88	0.93	0.91	0.91

287 considered to be satisfactory at all sites.

$$NSME = 1 - \frac{\sum_{i=1}^n (q_i - q_{iest})^2}{\sum_{i=1}^n (q_i - \bar{q})^2} \quad (15)$$

288 where n is the number of records in the validation data; q_i is the validation
 289 data; q_{iest} is the calculated result; \bar{q} is the average of the validation data.

290 After being validated, the CFD model predicted free surfaces are studied
 291 to investigate the impacts of tidal turbines on surface waves. For this purpose,
 292 an undisturbed case (i.e. no turbine) was run to provide baseline surface
 293 wave profiles. The computed free surfaces at the two time instants when the
 294 trough and peak pass the turbine location are presented in Figure 3 (A) and
 295 3 (B) respectively. It can be seen from Figure 3 that the inclusion of the
 296 rotor reduces the wave height; The wave height drops by $\sim 2.5\%$ when the
 297 rotor is present. It is also observed from Figure 3 that the wave length is
 298 increased due to the inclusion of the rotor.

299 The deformation of surface waves observed above, i.e. wave height drop
 300 and wave length increase, is likely to be caused by wave-current interactions.
 301 The obstruction effect of the rotor in motion forces the passing water to flow
 302 around the device, causing the velocity near the free surface to be increased.
 303 The accelerated flow at the surface results in a faster transport of wave energy
 304 and, consequently, reduced wave height and increased wave length.

305 4 Verification of the FVCOM model

306 This section explores the possibility of using the OBSTACLE mentioned
 307 above to represent the observed rotor-caused wave height drop. Hence, a
 308 FVCOM based model was set up according to the above-mentioned experi-
 309 mental conditions. The mesh of the model has a uniform spatial resolution of
 310 0.2 m (i.e. 1D) throughout the computational domain. Vertically, the water
 311 column is evenly divided into 50 sigma layers to accommodate the turbine
 312 representation in the current and turbulence modules recorded in [26].

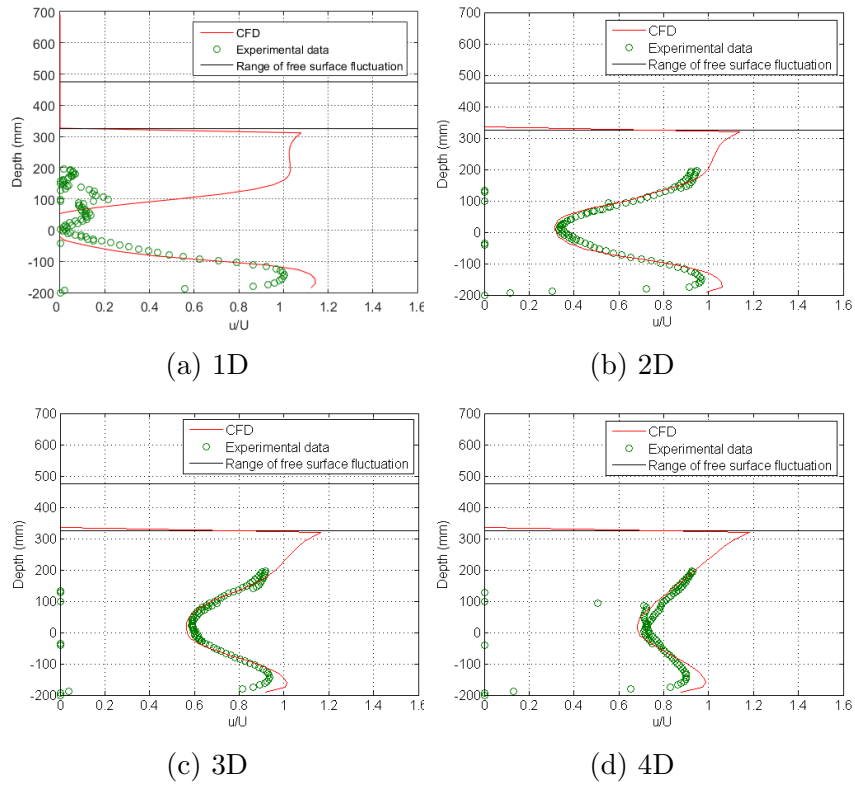


Figure 2: Normalized velocity profiles of the wave-current CFD case against those measured in the laboratory at 1D, 2D, 3D and 4D downstream of the rotor.

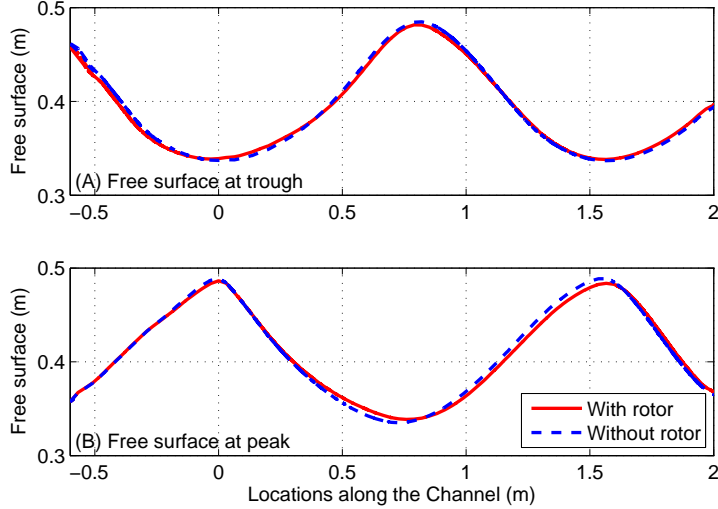


Figure 3: CFD predicted free surfaces at the wave trough (A) and peak (B) with and without the rotor. The rotor is positioned at 0 m along the channel.

313 The turbine effects on surface wave propagation is represented by sub-
 314 tracting a certain amount of energy from the energy conservation equation
 315 (Equation 14) as discussed in Section 2.4. In particular, the wave energy
 316 transmission coefficient K_t needs to be estimated. For this purpose, three
 317 cases are tested: baseline case where turbine is absent and the hydrodynam-
 318 ics resemble those of the undisturbed experimental conditions, case TNO
 319 where the turbine is present but OBSTACLE is deactivated, and case TYO
 320 where both the turbine and OBSTACLE are implemented. In case TYO, the
 321 wave energy transmission coefficient of OBSTACLE, K_t , is 0.98.

322 To verify the choice of K_t , Figure 4 compares the drop of wave height in
 323 percentage along the channel of the two FVCOM cases, TYO and TNO, and
 324 that of one of the CFD models (rotor positioned at 0.2 m above the bed).
 325 Wave height drop in percentage (hereafter wave height drop) is defined as the
 326 ratio between the decrease in wave height and the background wave height.
 327 It is obvious that the wave height drop at the turbine location predicted by
 328 TNO is $\sim 1.0\%$ less than that predicted by the corresponding CFD case. This
 329 difference is quite significant given that the correct drop is $\sim 2.5\%$ at the
 330 turbine location. The result of case TYO shows that the wave height drop is
 331 increased to the correct level by activating OBSTACLE; it is increased by \sim

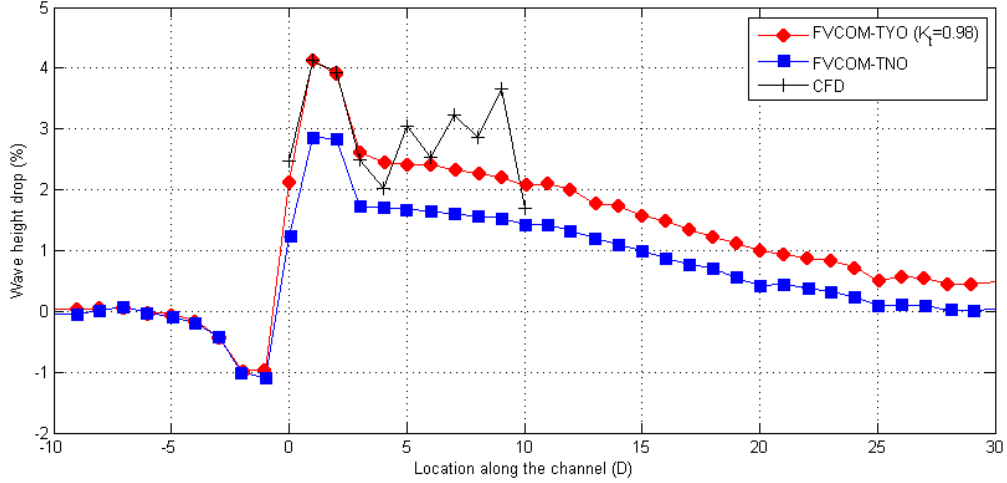


Figure 4: Wave height drop in terms of percentage along the channel for two FVCOM cases, TYO and TNO, and for the wave-current CFD case (the turbine is positioned at 0D).

332 0.9% at the turbine location due to the introduction of OBSTACLE. Hence,
 333 the built-in feature OBSTACLE provides an effective way to simulate the
 334 turbine-caused wave height reduction.

335 The consistency between the CFD and FVCOM simulated wave heights
 336 in the wake of the turbine is obtained through calibrating the wave energy
 337 transmission coefficient K_t mentioned in Section 2.4 according to the results
 338 of the CFD model. However, it should be noted that the two models are
 339 based on different wave theories: the CFD model uses linear wave theory
 340 while the wave model in FVCOM (i.e. SWAN) is a spectral wave model.
 341 The reason the above-mentioned match is achievable despite different wave
 342 theories are applied is that the action balance equation of SWAN (Equation
 343 14) is in fact an energy transfer equation derived based on the linear wave
 344 theory used in the CFD model. The spectrum which contains information
 345 of wave energy in different directions and frequencies can be regarded as a
 346 superposition of independent waves following the linear wave theory.

347 5 Application — Standalone turbine tests

348 This section investigates the effects of the inclusion of waves and activation of
349 OBSTACLE upon the bottom shear stress based on a series of tests carried
350 out using a prototype 15 m diameter turbine model as the test bed [26].
351 Water depth of these cases is 45 m and the turbine hub is located at a
352 depth of 22.5 m. The flow and wave conditions are set to reflect those of the
353 Anglesey coast, North Wales, UK, which is identified as one of the potential
354 locations for tidal energy exploitation [53]. The water velocity is 1.0 m/s.
355 The significant wave height is 2.4 m and wave period is 7 s: typical conditions
356 of storms observed along the Anglesey coast [54].

357 The results of a current-only case (case TbM (BBL)) and a wave-imposed
358 case without OBSTACLE (case TNO15) are compared to reveal the impact
359 of surface waves on bottom shear stress. Another wave-current coupled case
360 with OBSTACLE activated (case TYO15) is also tested in this section to
361 further discuss how OBSTACLE affects the prediction of bottom shear stress.
362 Turbine simulation in the current and turbulence modules is activated in
363 these cases according to [26]. Bottom shear stress of these three cases are
364 calculated through the BBL module [41] mentioned above. In case TYO15,
365 the OBSTACLE wave energy absorption line (Figure 1) is 15m long and K_t
366 is 0.98.

367 The computed significant wave height of cases TYO15 and TNO15 are
368 shown in Figure 5 (A). Figure 5 (B) & (C) show normalized water velocity
369 at the surface and bottom shear stress for cases TYO15, TNO15 and TbM
370 (BBL). It is observed from Figure 5 (A) that the inclusion of the turbine is
371 causing the significant wave height decrease by $\sim 4.7\%$ beyond 10D down-
372 stream of the turbine and the inclusion of OBSTACLE further reduces the
373 significant wave height by 0.6%.

374 In Figure 5 (B), velocity at the surface increases due to the implemen-
375 tation of the turbine; In this case a peak increase of $\sim 23\%$ is observed for
376 TYO15 1D downstream of the turbine. Further, velocity at the surface for
377 TNO15 is $\sim 4\%$ higher than TbM (BBL). This is due to the Stokes drift
378 caused by the waves [55]. Note that waves propagating in the same direction
379 of the carrying current are reported to cause a reduction of the flow velocity
380 near the surface [56]. The inclusion of OBSTACLE leads to a reduction in
381 wave height and hence an increase in flow velocity near the surface. This
382 leads to a surface velocity increase of $\sim 3\%$ for TYO15 over TNO15.

383 In Figure 5 (C), it is observed that the inclusion of surface waves increases

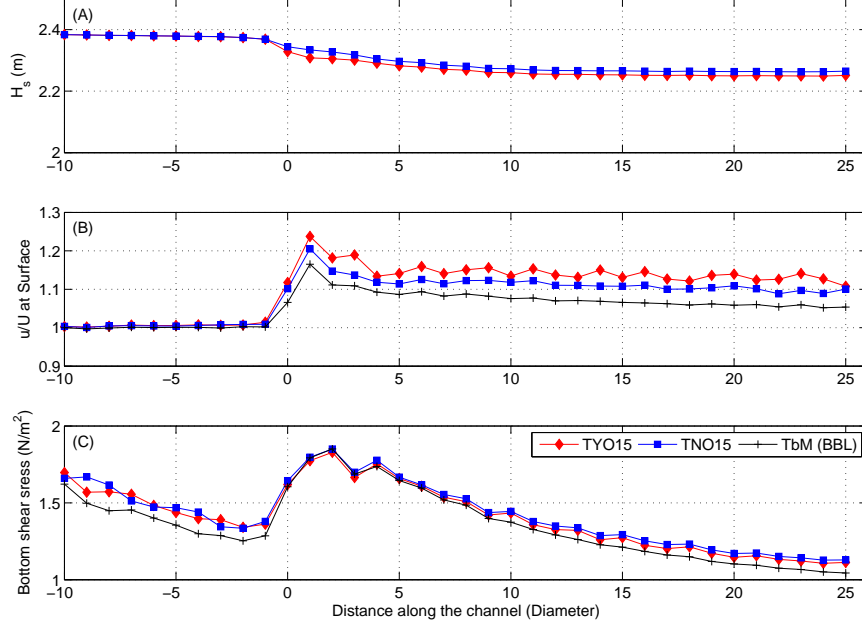


Figure 5: (A) Significant wave height (B) Normalized water velocity at the surface and (C) Bottom shear stress, all calculated under three different scenarios: TYO15 - Retarding force + turbulent terms + waves + obstacle, TNO15 - Retarding force + turbulent terms + waves and TbM (BBL) - Retarding force + turbulent terms with bottom shear stress calculated through BBL. (The turbine is positioned at 0D)

384 bottom shear stress by an average of $\sim 7\%$ (for both TYO15 and TNO15)
 385 in the regions upstream of the turbine and $>9D$ downstream of the turbine.
 386 Difference in bottom shear stress caused by the waves from the turbine within
 387 $9D$ downstream of the turbine is relatively small (compared to outside this
 388 region). The retarding force which represents the turbine operation is playing
 389 the major role within this region, increasing the bottom shear stress by $\sim 50\%$
 390 of all three cases. This is a result of the flow acceleration near the bed
 391 being identified by a three-dimensional model [26]. Also, the wave bottom
 392 boundary layer is likely to be dissipated by the strong mixing caused by the
 393 turbine. In the far wake region, as expected, the inclusion of OBSTACLE
 394 slightly reduces bottom shear stress compared to TNO15 ($\sim 2\%$ reduction).

395 6 Discussions

396 6.1 Choice of turbine simulation method in FLUENT

397 Apart from VBM, there are a number of other methods that are widely
398 used to model tidal turbines in CFD simulations, such as the Actuator
399 Disc Method (ADM) which provides a momentum sink in the rotor disk
400 fluid zone without the BEM [57], and the Moving Reference Frame (MRF)
401 method which explicitly simulate the structure and the rotational motion
402 of the turbine [58]. Compared to the fully resolved MRF, VBM has two
403 well-documented limitations: 1) The mechanical turbulence caused by the
404 turbine blades in the form of tip and hub vortex and the blade trailing edge
405 wake is not accounted for [59], leading to under-predicted turbulence level
406 behind the turbine [26]. 2) The lift and drag forces are annularly averaged
407 over a full rotation circle, hence the VBM does not account for transient flow
408 characteristics [10]. This could result in skipping of wave loadings on tur-
409 bines due to the fact that waves can have higher frequencies than the blade
410 passing frequency. Further, large shear can exist across the rotor depend-
411 ing on the vertical flow structure (especially when waves are present as the
412 effect of waves vary significantly with depth), suggesting that the annularly
413 averaged forces could be potentially invalid and a full multi-blade simulation
414 is required to resolve the loadings more realistically. These disadvantages
415 of VBM can result in fallacious power and fatigue analysis, which can ulti-
416 mately lead to inaccurate prediction of design, build and maintenance costs
417 [33]. However, considering that the main focus of this research is the impact
418 of turbines on waves, instead of waves on the performance of turbines, and
419 that the coefficients of VBM can be calibrated against measured data to en-
420 sure acceptable predicted flow conditions in the wake (e.g. [11, 26]), VBM is
421 a viable choice for the purpose of this research. It is also worth noting that
422 the integration of surface waves in CFD simulations can significantly increase
423 the computational effort required, hence VBM which is comparably less com-
424 putationally demanding can serve as a more feasible choice for wave-current
425 simulations, especially in cases where multiple devices are presented.

426 6.2 Effect of static turbine simulation coefficients

427 By using VBM to simulate turbines, the lift/drag coefficients ($c_{L,D}$) of the
428 turbine in the CFD simulations are assumed to be static despite the flow

429 conditions. This could be incorrect as surface waves can cause time-varying
430 loadings on turbines which in turn lead to time-dependent effective $c_{L,D}$ [33].
431 In terms of impact assessment, the fixed $c_{L,D}$ used in the CFD simulations
432 could lead to under-/over-estimated instantaneous flow deceleration, turbu-
433 lence generation, wave height modulation and bottom bed shear change.
434 Similarly, the coefficients related to turbine simulation in FVCOM (those in
435 current and turbulent mixing modules [26], as well as K_t in the wave mod-
436 ule mentioned above) are static. Hence, the FVCOM model could also lead
437 to the above-mentioned inaccurate instantaneous predictions. However, it is
438 worth noting that the assessment of turbine-driven local/regional morpholog-
439 ical evolution, which depend highly on the above-mentioned hydrodynamic
440 factors, should take into consideration the life span of tidal turbine arrays
441 which could be up to 100 years [60]. Therefore, the mean overall morpho-
442 logical evolution when considered over such a long time scale could become
443 insensitive to the individual predictions.

444 7 Conclusions

445 The impact of turbines on surface waves is investigated in this study in light
446 of the importance of surface waves on local/regional geomorphology and also
447 as a response to the lack of attention on turbine-induced wave dynamic al-
448 ternation in the literature. A CFD simulation with a turbine (blockage ratio
449 3.3% and TSR 5.5) located 0.4 m from the free surface revealed a $\sim 3\%$ re-
450 duction in wave height as well as a slight increase in wave length. To simulate
451 the wave height drop in FVCOM, the OBSTACLE energy dissipation routine
452 of the wave module (SWAN) was activated, and it captured the behaviour to
453 a large extent (Figure 4). However, there are two obvious shortcomings with
454 the modelling method. First, by simply using OBSTACLE which subtracts
455 energy from the propagating surface waves, the model does not fully resolve
456 the mechanism of turbine-wave interaction. In this regard, further work is
457 recommended into the investigation of how turbines and surface waves in-
458 teract. Second, only one turbine configuration is tested at a single depth.
459 However, the specific value of K_t may in fact need to be defined as a function
460 of depth which would also serve as an interesting avenue for investigation.

461 Impacts of tidal turbines on bed shear stress are also studied under wave-
462 current fully coupled scenarios. It is found that although the inclusion of
463 waves increased bed shear stress in the upstream area by an average of $\sim 7\%$,

464 its influence on the bottom shear stress within the near wake zone, i.e. 0D-
465 9D downstream of the turbine, is negligible. The turbine is the dominant
466 factor within this region that increases the bottom shear stress by $\sim 50\%$, as
467 the blockage effect of the turbine forces the water to flow around the device
468 which increases the water velocity near the bed and subsequently increases
469 the bottom shear stress. Impacts of waves on bottom shear stress resume
470 in the far wake, i.e. $>9D$ downstream of the turbine. The influence of
471 OBSTACLE on bottom shear stress is also noticeable in the far wake. The
472 OBSTACLE implemented in this work reduced bottom shear stress by $\sim 2\%$.

473 Acknowledgement

474 X. Li would like to acknowledge support from the Chinese Scholar Council
475 and the University of Liverpool. Dr. Sufian also provided the settings for
476 VBM in ANSYS FLUENT. The authors are grateful to Brendan Murphy for
477 his help setting-up and running the experiments. The authors would also like
478 to acknowledge funding from the Engineering and Physical Sciences Research
479 Council (EPSRC) to grant EP/J010359/1 (Interactions of flow, tidal stream
480 turbines and local sediment bed under combined waves and tidal conditions),
481 which is part of the Supergen consortium.

482 References

- 483 [1] L. Myers, A. Bahaj, An experimental investigation simulating flow ef-
484 fects in first generation marine current energy converter arrays, *Renew-
485 able Energy* 37 (1) (2012) 28–36.
- 486 [2] L. Myers, A. Bahaj, Experimental analysis of the flow field around hor-
487 izontal axis tidal turbines by use of scale mesh disk rotor simulators,
488 *Ocean Engineering* 37 (2) (2010) 218–227.
- 489 [3] F. Maganga, G. Germain, J. King, G. Pinon, E. Rivoalen, Experimental
490 characterisation of flow effects on marine current turbine behaviour and
491 on its wake properties, *IET Renewable Power Generation* 4 (6) (2010)
492 498–509.
- 493 [4] S. Tedds, I. Owen, R. Poole, Near-wake characteristics of a model hori-
494 zontal axis tidal stream turbine, *Renewable Energy* 63 (2014) 222–235.

- 495 [5] L. B. Jordan, S. Simmons, S. McLelland, B. Murphy, D. Parsons, L. Vy-
496 bulkova, The impact of tidal stream turbines on 3D flow and bed shear
497 stress measured with particle image velocimetry in a laboratory flume,
498 in: Proceedings of the 11th European Wave and Tidal Energy Confer-
499 ence, Nantes, France, 2015, pp. 654–660.
- 500 [6] A. Olczak, T. Stallard, P. Stansby, Tidal turbine wake recovery due to
501 turbulent flow and opposing waves, Proceedings of the 2nd Oxford tidal
502 energy workshop.
- 503 [7] X. Sun, J. Chick, I. Bryden, Laboratory-scale simulation of energy ex-
504 traction from tidal currents, *Renewable Energy* 33 (6) (2008) 1267–1274.
- 505 [8] M. Harrison, W. Batten, L. Myers, A. Bahaj, Comparison between CFD
506 simulations and experiments for predicting the far wake of horizontal
507 axis tidal turbines, *IET Renewable Power Generation* 4 (6) (2010) 613–
508 627.
- 509 [9] L. Bai, R. R. Spence, G. Dudziak, Investigation of the influence of array
510 arrangement and spacing on tidal energy converter (TEC) performance
511 using a 3-dimensional CFD model, in: Proceedings of the 8th European
512 Wave and Tidal Energy Conference, Uppsala, Sweden, 2009, pp. 654–
513 660.
- 514 [10] X. Bai, E. Avital, A. Munjiza, J. Williams, Numerical simulation of a
515 marine current turbine in free surface flow, *Renewable Energy* 63 (2014)
516 715–723.
- 517 [11] R. Malki, I. Masters, A. J. Williams, T. N. Croft, Planning tidal
518 stream turbine array layouts using a coupled blade element momentum–
519 computational fluid dynamics model, *Renewable Energy* 63 (2014) 46–
520 54.
- 521 [12] A. Goude, O. Ågren, Simulations of a vertical axis turbine in a channel,
522 *Renewable energy* 63 (2014) 477–485.
- 523 [13] A. F. Shchepetkin, J. C. McWilliams, The regional oceanic model-
524 ing system (ROMS): a split-explicit, free-surface, topography-following-
525 coordinate oceanic model, *Ocean Modelling* 9 (4) (2005) 347–404.

- 526 [14] C. Chen, H. Liu, R. C. Beardsley, An unstructured grid, finite-volume,
527 three-dimensional, primitive equations ocean model: application to
528 coastal ocean and estuaries, *Journal of atmospheric and oceanic tech-*
529 *nology* 20 (1) (2003) 159–186.
- 530 [15] I. G. Bryden, S. J. Couch, ME1 marine energy extraction: tidal resource
531 analysis, *Renewable Energy* 31 (2) (2006) 133–139.
- 532 [16] R. Karsten, J. McMillan, M. Lickley, R. Haynes, Assessment of tidal
533 current energy in the Minas Passage, Bay of Fundy, *Proceedings of*
534 *the Institution of Mechanical Engineers, Part A: Journal of Power and*
535 *Energy* 222 (5) (2008) 493–507.
- 536 [17] I. Walkington, R. Burrows, Modelling tidal stream power potential, *Ap-*
537 *plied Ocean Research* 31 (4) (2009) 239–245.
- 538 [18] Z. Defne, K. A. Haas, H. M. Fritz, Numerical modeling of tidal currents
539 and the effects of power extraction on estuarine hydrodynamics along
540 the Georgia coast, USA, *Renewable Energy* 36 (12) (2011) 3461–3471.
- 541 [19] R. Ahmadian, R. Falconer, B. Bockelmann-Evans, Far-field modelling
542 of the hydro-environmental impact of tidal stream turbines, *Renewable*
543 *Energy* 38 (1) (2012) 107–116.
- 544 [20] D. R. Plew, C. L. Stevens, Numerical modelling of the effect of turbines
545 on currents in a tidal channel—Tory Channel, New Zealand, *Renewable*
546 *Energy* 57 (2013) 269–282.
- 547 [21] D. Fallon, M. Hartnett, A. Olbert, S. Nash, The effects of array configu-
548 ration on the hydro-environmental impacts of tidal turbines, *Renewable*
549 *Energy* 64 (2014) 10–25.
- 550 [22] J. Thiébot, P. B. du Bois, S. Guillou, Numerical modeling of the effect of
551 tidal stream turbines on the hydrodynamics and the sediment transport—
552 Application to the Alderney Race (Raz Blanchard), France, *Renewable*
553 *Energy* 75 (2015) 356–365.
- 554 [23] R. Martin-Short, J. Hill, S. Kramer, A. Avdis, P. Allison, M. Piggott,
555 Tidal resource extraction in the Pentland Firth, UK: Potential impacts
556 on flow regime and sediment transport in the Inner Sound of Stroma,
557 *Renewable Energy* 76 (2015) 596–607.

- 558 [24] P. E. Robins, S. P. Neill, M. J. Lewis, Impact of tidal-stream arrays in
559 relation to the natural variability of sedimentary processes, *Renewable*
560 *Energy* 72 (2014) 311–321.
- 561 [25] T. Roc, D. C. Conley, D. Greaves, Methodology for tidal turbine rep-
562 resentation in ocean circulation model, *Renewable Energy* 51 (2013)
563 448–464.
- 564 [26] X. Li, M. Li, S. J. McLelland, L.-B. Jordan, S. M. Simmons, L. O.
565 Amoudry, R. Ramirez-Mendoza, P. D. Thorne, Modelling tidal stream
566 turbines in a three-dimensional wave-current fully coupled oceanographic
567 model, *Renewable Energy* 114 (2017) 297–307.
- 568 [27] G. McCann, Tidal current turbine fatigue loading sensitivity to waves
569 and turbulence—a parametric study, in: *Proceedings of the 7th European*
570 *Wave and Tidal Energy Conference*, Porto, Portugal, 2007.
- 571 [28] G. McCann, M. Thomson, S. Hitchcock, Implications of site-specific
572 conditions on the prediction of loading and power performance of a
573 tidal stream device, in: *2nd International Conference on Ocean Energy*,
574 Brest, France, 2008.
- 575 [29] C. Faudot, O. G. Dahlhaug, Prediction of wave loads on tidal turbine
576 blades, *Energy Procedia* 20 (2012) 116–133.
- 577 [30] E. E. Lust, L. Luznik, K. A. Flack, J. M. Walker, M. C. Van Ben-
578 them, The influence of surface gravity waves on marine current turbine
579 performance, *International Journal of Marine Energy* 3 (2013) 27–40.
- 580 [31] L. Luznik, K. A. Flack, E. E. Lust, K. Taylor, The effect of surface waves
581 on the performance characteristics of a model tidal turbine, *Renewable*
582 *energy* 58 (2013) 108–114.
- 583 [32] T. de Jesus Henriques, S. Tedds, A. Botsari, G. Najafian, T. Hedges,
584 C. Sutcliffe, I. Owen, R. Poole, The effects of wave–current interaction on
585 the performance of a model horizontal axis tidal turbine, *International*
586 *Journal of Marine Energy* 8 (2014) 17–35.
- 587 [33] M. A. Holst, O. G. Dahlhaug, C. Faudot, Cfd analysis of wave-induced
588 loads on tidal turbine blades, *IEEE Journal of Oceanic Engineering*
589 40 (3) (2015) 506–521.

- 590 [34] T. Spencer, I. Möller, F. Rupprecht, T. Bouma, B. Wesenbeeck,
591 M. Kudella, M. Paul, K. Jensen, G. Wolters, M. Miranda-Lange, et al.,
592 Salt marsh surface survives true-to-scale simulated storm surges, *Earth*
593 *Surface Processes and Landforms* 41 (4) (2016) 543–552.
- 594 [35] L. C. Van Rijn, L. C. van Rijn, L. C. van Rijn, *Principles of sediment*
595 *transport in rivers, estuaries and coastal seas*, Vol. 1006, Aqua publica-
596 tions Amsterdam, 1993.
- 597 [36] M. S. Longuet-Higgins, Longshore currents generated by obliquely inci-
598 dent sea waves: 1, *Journal of geophysical research* 75 (33) (1970) 6778–
599 6789.
- 600 [37] N. C. Kraus, S. Harikai, Numerical model of the shoreline change at
601 oarai beach, *Coastal Engineering* 7 (1) (1983) 1–28.
- 602 [38] I. Fluent, *Fluent users guide* (2006).
- 603 [39] T. Hedges, Regions of validity of analytical wave theories, *Oceanog-*
604 *raphic Literature Review* 1 (43) (1996) 10.
- 605 [40] X. Li, 3D modelling of tidal stream energy extraction for impact assess-
606 ment, Ph.D. thesis, School of Engineering, University of Liverpool (9
607 2016).
- 608 [41] C. Chen, G. Cowles, R. Beardsley, An unstructured grid, finite-volume
609 coastal ocean model: FVCOM user manual, *SMASST/UMASSD*.
- 610 [42] N. Booij, R. Ris, L. H. Holthuijsen, A third-generation wave model for
611 coastal regions: 1. model description and validation, *Journal of Geo-*
612 *physical Research: Oceans* (1978–2012) 104 (C4) (1999) 7649–7666.
- 613 [43] J. C. Warner, C. R. Sherwood, R. P. Signell, C. K. Harris, H. G. Arango,
614 Development of a three-dimensional, regional, coupled wave, current,
615 and sediment-transport model, *Computers & Geosciences* 34 (10) (2008)
616 1284–1306.
- 617 [44] O. S. Madsen, Spectral wave-current bottom boundary layer flows,
618 *Coastal Engineering Proceedings* 1 (24).
- 619 [45] G. Mellor, The three-dimensional current and surface wave equations,
620 *Journal of Physical Oceanography* 33 (9) (2003) 1978–1989.

- 621 [46] G. Mellor, Some consequences of the three-dimensional current and sur-
622 face wave equations, *Journal of Physical Oceanography* 35 (11) (2005)
623 2291–2298.
- 624 [47] G. L. Mellor, M. A. Donelan, L.-Y. Oey, A surface wave model for cou-
625 pling with numerical ocean circulation models, *Journal of Atmospheric*
626 *and Oceanic Technology* 25 (10) (2008) 1785–1807.
- 627 [48] SWANTeam, SWAN Cycle III version 40.51 user manual, Delft Uni-
628 versity of Technology, Faculty of Civil Engineering and Geosciences,
629 Environmental Fluid Mechanics Section (2006).
- 630 [49] S. Sufian, Numerical modeling of impacts from horizontal axis tidal tur-
631 bines, Ph.D. thesis, School of Engineering, University of Liverpool (6
632 2016).
- 633 [50] D. Maréchal, A soil-based approach to rainfall-runoff modelling in un-
634 gauged catchments for england and wales.
- 635 [51] J. Allen, P. Somerfield, F. Gilbert, Quantifying uncertainty in high-
636 resolution coupled hydrodynamic-ecosystem models, *Journal of Marine*
637 *Systems* 64 (1-4) (2007) 3–14.
- 638 [52] L. Xiaorong, A. Plater, N. Leonardi, Modelling the transport and export
639 of sediments in macrotidal estuaries with eroding salt marsh, *Estuaries*
640 *and Coasts* (2018) 1–14.
- 641 [53] A. Iyer, S. Couch, G. Harrison, A. Wallace, Variability and phasing of
642 tidal current energy around the United Kingdom, *Renewable Energy* 51
643 (2013) 343–357.
- 644 [54] M. Lewis, S. Neill, M. Hashemi, M. Reza, Realistic wave conditions and
645 their influence on quantifying the tidal stream energy resource, *Applied*
646 *Energy* 136 (2014) 495–508.
- 647 [55] K. E. Kenyon, Stokes drift for random gravity waves, *Journal of Geo-*
648 *physical Research* 74 (28) (1969) 6991–6994.
- 649 [56] M. Olabarrieta, R. Medina, S. Castanedo, Effects of wave–current inter-
650 action on the current profile, *Coastal Engineering* 57 (7) (2010) 643–655.

- 651 [57] L. Lavaroni, S. J. Watson, M. J. Cook, M. R. Dubal, A comparison of
652 actuator disc and bem models in cfd simulations for the prediction of
653 offshore wake losses, in: *Journal of Physics: Conference Series*, Vol. 524,
654 IOP Publishing, 2014, p. 012148.
- 655 [58] T. ODoherty, A. Mason-Jones, D. ODoherty, C. Byrne, I. Owen,
656 Y. Wang, Experimental and computational analysis of a model hori-
657 zontal axis tidal turbine, in: *8th European Wave and Tidal Energy*
658 *Conference (EWTEC)*, Uppsala, Sweden, 2009.
- 659 [59] T. Burton, D. Sharpe, N. Jenkins, E. Bossanyi, *Wind energy handbook*,
660 John Wiley & Sons, 2001.
- 661 [60] S. Walker, R. Howell, P. Hodgson, A. Griffin, Tidal energy machines: A
662 comparative life cycle assessment study, *Proceedings of the Institution of*
663 *Mechanical Engineers, Part M: Journal of Engineering for the Maritime*
664 *Environment* 229 (2) (2015) 124–140.